CHRISTIAN-ALBRECHTS-UNIVERSITÄT ZU KIEL

MASTER THESIS

Thesis Title

Author:
Anne Fischer

Supervisor:
Prof. Dr.
Wimmer-Schweingruber

Research Group Name
Department or School Name

November 27, 2019

Abstract

The Thesis Abstract is written here (and usually kept to just this page). The page is kept centered vertically so can expand into the blank space above the title too...

Contents

Chapter 1

Motivation

10

Chapter 2

Pickup Ions

Pickup ions are created when neutral atoms inside the heliosphere become ionised and are subsequently swept away with the heliospheric magnetic field that is embedded within the solar wind.

2.1 The Heliosphere / Introduction

Oder Überkapitel Solar Physics?

Heliosphere: Grenze zu LISM

Solar Wind: Zusammensetzung, schneller und langsamer, high latitudes: less complex, constant in speed

B-Feldgleichung

Irgendwohin muss unbedingt Motivation, warum PUIs überhaupt interessant sind zu messen!
PU Process

2.2 Pickup Ions

A neutral atom inside the heliosphere is only subjected to the gravitational force and radiation pressure of the sun. It is not sensitive to any electromagnetic forces until it becomes ionised by solar ultra-violet radiation, charge exchange with solar wind protons or electron impact (Q?). After ionisation the particle starts interacting with the solar wind plasma. In particular it is forced onto a gyro orbit about the heliospheric magnetic field that is embedded within the solar wind. As the freshly created ion is swept away with the magnetic field line it is "picked up" from its location of ionisation – a new pickup ion (PUI) has been created.

PUIs were first observed by Möbius et al. (1985) with the SULEICA Instrument on the AMPTE spacecraft. The particles measured at 1 AU were He+ ions of interstellar origin.

Once the particle is ionised, its probability to become ionised another time decreases (Quelle). This characteristic of being only singly charged can help to discriminate PUIs from solar wind ions, that are mostly more often charged (Q?).

PUIs are mostly only single charged. This characteristic can help to distinguish them

from solar wind ions of coronal origin which often have been ionized multiple times, if not completely. (Q?)
VDF non-maxwellian, spatial density pattern

There have been observed several species of PUIs:

2.3 Interstellar Pickup Ions

Heliosheath, relative motion

The neutral part of the LISM can enter the heliosphere as it is not affected by the heliosheath (Todo). Inside the heliosphere the neutrals are guided only by the gravitational force and raOriginofC-Geissdiation pressure of the sun. The neutral particle's species determines how deep it can travel into the heliosphere before it becomes ionized. Species with a higher First Ionization Potential will be able to approach the sun much closer without being ionized. This results in He+ being the dominant PUI species at a solar distance of 1 AU even if in the LISM the abundance of hydrogen is about 10 times the one of helium.

- ionisation process is also dependent on the species
- radiation pressure only important for H (and He?). Kepler orbit...
- Spatial distribution:
  gravitational force and radiation pressure lead to two regions of enhanced density of neutrals (in the ecliptic): Focusing cone and crescent. Focusing cone: For species with high FIP (as the others are ionized before and do not reach the downwind side of the sun)
- variation of He+ with the solar cycle: Rucinski 2003
- H, O and N are depleted in the filtration region (Baranov Malama 1995), Wimmer Skript: even before ioniztion: density is determined by ratio of gravitational force and photon pressure
- neutral density determines PUI production rate

2.4 Inner-source Pickup Ions

The idea of an additional source for the PUI's neutral seed population was born when Geiss, Gloeckler, Fisk, et al. (1995) measured a global distribution of C+ PUIs with the SWICS instrument on Ulysses. Interstellar carbon exists almost exclusively in a single charged state (Frisch et al., 2011) in the LISM. As only neutral atoms can enter the heliosphere it was not expected to find a distinct signature of C+ pickup ions. However, pickup carbon was observed with about the same ratio as oxygen, of which, in contrast, 80% is in a neutral charge state in the interstellar medium. These findings suggested that there must be another source for neutrals that has its origin somewhere inside the heliosphere.
In following studies (e.g. Geiss, Gloeckler, and Steiger, 1995) there were found also other species like O+ and Ne+ of these, so called, inner-source PUIs.
Inner-source PUIs show a composition that is similar to the one of the solar wind

(Gloeckler et al., 2000; Allegrini et al., 2005) as well as a velocity distribution function that is centered around $w_{SC} \approx 1$ (Schwadron et al., 2000) and seems to have thermalized with the solar wind.
Beneath those two characteristics there are other aspects concerning inner-source PUIs, that are still under debate. In particular that is the production mechanism of their neutral seed population. Allegrini et al. (2005) has summarized current candidates for possible scenarios. Two of those give an explanation for the ion's composition as they directly incorporate solar wind ions in the process:

- Solar wind recycling (Gloeckler et al., 2000; Schwadron et al., 2000): Absorption of solar wind ions by heliospheric grains and subsequent reemission of neutral atoms
- Solar wind neutralization (Wimmer-Schweingruber and Bochsler, 2002): Solar wind ions penetrate sub-micron-sized dust grains and undergo (partial) neutralization by charge exchange

(As this work does not focus on inner-source PUIs in particular...)

2.5 VDF

After the particle has been ionised it is forced onto a gyro motion about the local field line of the heliospheric magnetic field due to the Lorentz force.

To examine the velocity distribution of PUIs after they have been ionized we need to consider the initial speed v_{ini} of the neutral particle. For neutrals from the LISM this is mainly given by the inflow speed v_{ISM} of the local interstellar medium with which they enter the heliosphere. As we don't exactly know about the production mechanism of inner-source PUIs, the following considerations mainly relate to interstellar PUIs. Schwadron et al. (2015) obtained $v_{ISM} \approx 25\,\mathrm{km\,s^{-1}}$ with the IBEX satellite for helium. Considering the acceleration by the sun's gravitational force we have a maximum initial speed of $v_ini \approx 50\,\mathrm{km\,s^{-1}}$ at 1 AU. Compared to an average solar wind speed of $v_{sw} \approx 400\,\mathrm{km\,s^{-1}}$ one can neglect this initial speed in a first step.

For simplicity we thus consider a neutral particle at rest that becomes ionized by one of the aforementioned processes. The freshly created ion now is subjected to the electromagnetic forces of the solar wind plasma. In particular, it finds itself at a velocity v_{sw} relative to the magnetic field which is convected outwards by the solar wind that is assumed to flow radially outwards. Due to the Lorentz force the PUI starts to gyrate about the magnetic field line on an orbit that is perpendicular to it.
When we further consider a magnetic field's orientation that is perpendicular to the solar wind flow, $\vec{B} \perp \vec{v}_{sw}$, the ion's gyration speed is v_{sw} while its guiding center moves together with the field line at a speed of v_{sw} as well. Thus, the total speed of the PUI ranges between $0\,\mathrm{v_{sw}}$ and $2\,\mathrm{v_{sw}}$ in a sun frame of reference.
As the heliospheric magnetic field lines are shaped like an Archimedean spiral, the so called *Parker spiral*, the assumption of a perpendicular magnetic field only applies when solar wind speed v_{sw} and solar distance $r_\odot$ follow the relation

$$90^\circ \approx arctan\left(\frac{2\pi}{T_\odot \cdot v_{sw}} r_\odot\right)$$

with sun's sidereal period $T_\odot \approx 25\,d$ (Prölss, 2004). In other cases, e.g. for solar distances about 1 AU, at which the angle between solar wind and magnet field direction

is approximately 45°, the maximum speed in a sun frame of reference is decreased. In general, the gyration speed is given by

todo

with ... .

The velocity space for a pickup situation with a non-radial magnetic field orientation is shown in figure todo on the right. The PUI's total velocity consists of the movement of the guiding center (...) and the gyration velocity (...). We note, that in this case there is a relative velocity between the motion of the solar wind bulk and the PUI's guiding center movement.
However, independent on the magnetic field orientation, every possible velocity space trajectory is part of a sphere with the radius v_{sw} centered around $\vec{v}_{sw}$. That means that, in the frame of the solar wind, the freshly created PUI always moves with a speed that is as fast as the solar wind itself. (todo: Hier w einführen?)

Instead of a single PUI we can consider an ensemble of PUI's that is injected into the solar wind while the magnetic field orientation is not changing much. For that we expect the VDF to form a ring shape in velocity space, commonly called the "PUI torus VDF" (Oka et al., 2002). The expected orientation of this highly anisotropic torus VDF depends on the local magnetic field direction and is sketched in figure todo for three different angles.

...thickness that is related (associated) to the neutral's velocity and is very small compared to the radius...

Spatial diffusion: chalov Fahr 1998. Signature of plasma parcel in which is was produced doesn't match with the one it is measured in

After the injection, the PUI population is radially carried away with the solar wind. During phase space transport through the heliosphere the PUIs are subjected to multiple processes that are expected to modify the shape of the initial toroidal VDF. However, it is not completely understood how the VDF evolves in detail.

A fast isotropization of the VDF due to pitch-angle scattering was suggested by Vasyliunas and Siscoe (1976) in a theoretical work. However, observations by e.g. Möbius et al. (1998) on $He+$ or Gloeckler et al. (1995) on TODO have shown clear anisotropic features in the measured VDFs. Following studies (todo) explained these findings with the assumption that the ions would be injected into the sunward hemisphere of velocity space more likely. Ineffective pitch-angle scattering into the anti-sunward hemisphere thus would result in an radial anisotropy.

Recent observations have emphasized the influence of the magnetic field direction on the measured anisotropy. Utilising 2D analyses of the velocity space, Oka et al. (2002) and Drews et al. (2015) found that the measured VDF of PUIs is systematically oriented about the direction that is perpendicular to the magnetic field. Thus, it is believed that the VDF's anisotropic features are remnants of the initial toroidal VDF. (and the pa scattering didnt have enough time to isotropize the distribution)

Furthermore, there are different acceleration and deceleration processes that change

the PUI's initial VDF and lead to a diffusion in velocity space. Under the assumption of an isotropic VDF the PUI population is often treated as an adiabatic gas that is consequently cooled when expanding with the solar wind. This picture, initially suggested by Vasyliunas and Siscoe (1976), however, must be reviewed due to the doubtful fact of a fully isotropic VDF. Another cooling mechanism, called the *magnetic cooling*, is due to the magnetic field weakening with solar distance. As the PUIs are swept outwards both their ... and their ...invariant have to be conserved which leads to a decrease in both velocity components (parallel and perpendicular to the magnetic field) and thus to a decrease in total velocity (in the frame of the solar wind).

(focusing (adiabatic invariant) & Ginzberg Landau (Fahr2008): "magnetic cooling" (auch gute Erklärung: Fahr&Fichtner2011))

Acceleration of PUIs can be caused by acceleration: first and seconf order fermi (verstehen, gründe): eher außen bzw. ehr innen. Außerdem ein Mechanismus, der nicht an einzelne Events gebunden ist, sondern immer vorhanden: Mechanismus für alle Teilchen, power law -5...
man kann in der 1D Verteilung beobachten, dass 2vsw exceeded wird

PUI He should be measured throughout the mission as they penetrate the heliosphere until 0.5 AU (Gloeckler et al., 1992)

Instrument that is capable of measuring this distribution: large acceptance in absolute velocity, large variation and resolution in angles

2.5.1 1D reduced VDF, aim of this work...?

Chapter 3

Instrumentation

3.1 Ulysses

The Ulysses spacecraft (Wenzel et al., 1992) was launched in 1990 and orbited the sun for nearly 20 years as a joint ESA/NASA project. Ulysses' most remarkable feature is its out-of-ecliptic orbit with an maximum heliographic latitude of 80.1 °. As the first spacecraft it was hence capable of taking in situ measurements from above the poles of the sun.

Thus, the primary goal of the mission was to study the heliosphere in three dimensions. In detail some of the original main objectives were:

- to study the interplanetary magnetic field and the solar wind, especially its composition, the origin and waves and shocks within the solar wind plasma
- to investigate galactic cosmic rays and energetic particles
- to improve the knowledge about interplanetary dust
- to explore the neutral component of interstellar gas

Some secondary objectives included e.g. the investigation of Jupiter's magnetosphere during the Jupiter flyby and the search for gravitational waves and for gamma-ray burst sources (Wenzel et al., 1992).
For these aims Ulysses was equipped with a wide range of different instruments and antennas. One of the in situ instruments is the Solar Wind Ion Composition Spectrometer, that will be described in the next chapter.

A sketch of Ulysses unique orbit is shown in figure 3.1. Ulysses was launched in October 1990 and left earth's gravitational field with 15.4 km/s. Starting with a flyby maneuver around Jupiter Ulysses was sent onto its highly elliptical orbit. With an orbital period of 6.2 years Ulysses completed nearly three orbits around the sun until communication was shut down in June 2009 due to the expiring of the radioisotope thermal generators. Within the mission's long lifetime the Sun's behaviour over its activity cycle of 22 years could be studied.

eccentricity, elliptical orbit...

aspect angle (antenna)– Power: RHU because too far away for solar panels (and radiation belt of Jupiter) – rotation stabilization – mission was extended multiple times

Abbildung Sun Cycles?

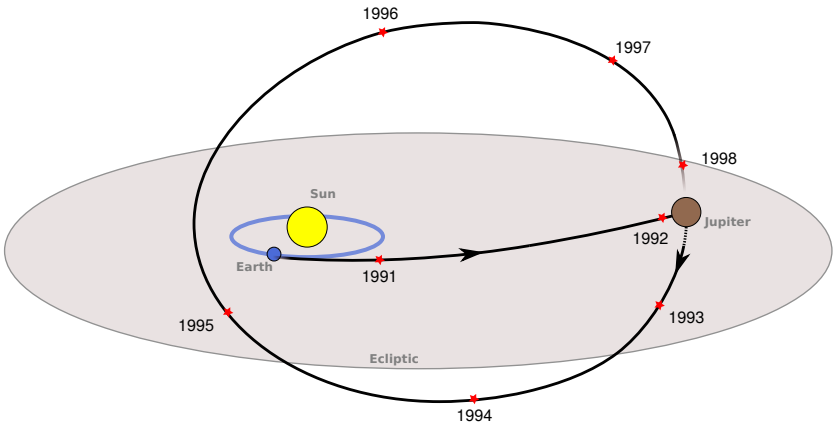

FIGURE 3.1: A sketch of Ulysses' first orbit. After the launch from earth in 1990 the spacecraft was sent to Jupiter from where it left the ecliptic on an elliptical orbit around the sun with perihelion at 1.3 AU and aphelion at 5.4 AU. Due to the orbit's high latitude of $\sim 80^\circ$ Ulysses crosses the Sun's pole regions two times between 1994 and 1996. Figure after European Space Agency (2019).

spinstabilisiert, Antenna fast Rotationsachse, Antenne zeigt zur Erde, woher Daten (Ulysses, SWICS, Erde)

Rotation

Importance PUIs: ref to PUI-Kapitel und zu objectives

3.2 SWICS

3.2.1 Introduction and Objectives

The Solar Wind Ion Composition Spectrometer (SWICS, Gloeckler et al. (1992)) is a time-of-flight mass spectrometer mounted on the spacecraft Ulysses (s. section 3.1). The instrument is designed to determine the elemental and charge-state composition and the velocity distribution of solar wind ions. With an energy-per-charge range from 0.16 keV/e to 59.6 keV/e SWICS is in principle able to measure every solar wind ion species from protons to iron with any typical charge state. Depending on the individual ion, energies from $E < 1$ keV up to $E > 1$ MeV are covered.

Additionally, the flight spare of SWICS has been mounted on the spacecraft ACE (TODO: ref Stone 1998)

Also capable of measuring PUIs! Erstmals gesehen...?

SWICS measures the mass m, the charge q and the energy E_{SSD} of entering ions by a combination of three separate measurements: The *electrostatic deflection analyzer* within SWICS entrance systems is used for determining the energy per charge of a particle. Within the time-of-flight/energy section the particle's time-of-flight (ToF) and energy (E_{SSD}) are measured.
Todo: Bild von SWICS, neben den beiden sieht man noch die Elektronik...

mounted on the sun-facing side of Ulysses

Opening angles: ± 2 deg perp, 90 deg parallel

In the following section the measurement is described in more detail.

3.2.2 Principle of Measurement / Identification of Particles

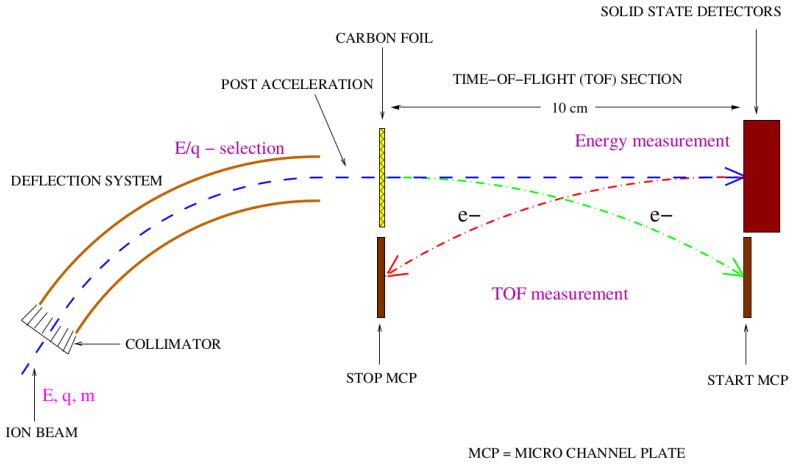

FIGURE 3.2: test

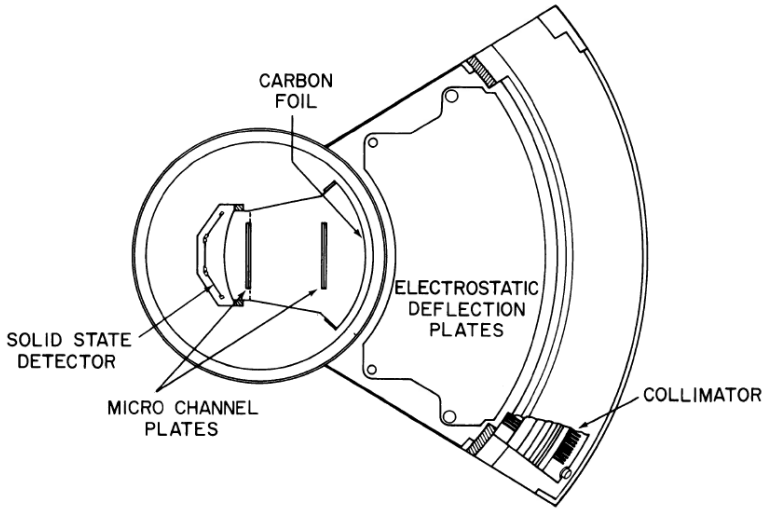

FIGURE 3.3: test

Collimator and Electrostatic Analyzer

Particles enter the instrument through the entrance collimator. It restricts particles to the ones with a trajectory that is parallel to the collimator slits. The geometry of the collimator is curved "fan-shaped"...TODO: Kollimatorgeometrie beschreiben Within the TODO: Two sections After the collimator particles have to pass the electrostatic analyzer. It is split up into two sections – energies from 0.16 to 14 keV/e are

covered by the proton/helium channel. Particles within this range of energy will be filtered by their EpQ and after an post-acceleration will be counted by a solid-state detector. As this simple measurement principle is very limiting for our analysis we will focus on the main channel that is suitable for a full m-vs.-mpq analysis. The main channel covers an EpQ range of 0.65 to 60 keV/e. A particle can only pass through the pair of curved deflection plates if its kinetic energy per charge equals a certain ratio that is given by the voltage between the two plates. To measure particles of different EpQ the deflection voltage is stepped through 64 logarithmically spaced values from TODO to TODO. As the voltage steps once per spin of Ulysses (every 12 seconds), a complete voltage cycle lasts $\sim$ 12.8 minutes. Every step has a relative uncertainty of $\Delta E/q \approx 5\%$ that is due to the finite space between the plates. TODO: Plot

Time-of-flight measurement

After passing the electrostatic analyzer ions are post-accelerated by an constant potential drop of 30 kV. They enter the ToF chamber with penetrating through a thin ($\sim 3\,\mu g/cm^2$) carbon foil where secondary electrons are emitted. These electrons are guided to a microchannel plate detector where a start signal is triggered. The stop signal is triggered after the particles have traversed a distance of 10 cm and hit one of the solid state detectors, where secondary electrons are emitted again. By combining the time stamps of the start and the stop signal the particle's ToF has been measured.

Energy measurement

Furthermore, the particle's energy is measured when they hit one of the three solid state detectors (SSD). The detectors have each an active area of $1.5x1.3\,cm^2$ and their orientation of the detectors can be seen in TODO. While the central detector is aligned perpendicular to the symmetry axis of SWICS, the other two detectors are slightly tilted with respect to this axis. Particles with different angles of incidence along the width of the collimator can be detected this way.

Thus, a wide field-of-view is provided, allowing measurements of particles, die schief reinkommen. Das passt zur Begrenzung vom Kollimator. Man kann auch unterscheiden, welcher getroffen wurde.
Verfälschungen? Folie etc?
The measured energy E_{SSD} is often referred to as *residual energy* in literature. This is potentially misleading as the particles might have more energy due to the post-acceleration

One of SWICS' main objectives is the measurement of the composition of incident particles. An ion and its charge state can be fully identified with the knowledge of its mass m and its mass-per-charge mpq. With the measurement of the ToF, the energy E_{SSD} and the knowledge of the EpQ-step we can calculate the mass, mpq and

velocity of an ion i with the following set of equations:

$$m_i = 2\,E_{SSD}\left(\frac{Tof}{d}\right)^2 \tag{3.1}$$

$$\frac{m_i}{q_i} = 2\,(EpQ + V_{PAC}) * \left(\frac{Tof}{d}\right)^2 \tag{3.2}$$

$$v_i = \sqrt{2\,EpQ\,\frac{q_i}{m_i}}, \tag{3.3}$$

where d is the length of the time-of-flight section and V_{PAC} is the post-acceleration voltage. v denotes the ion's initial velocity when entering the instrument and is not to be confused with its velocity during the time-of-flight measurement, that is altered particularly by the p ost-acceleration.

HISCALE: "The experiment provides information about the spatial origin of events by treating each spin as eight sectors of approximately equal duration."

Chapter 4

Data Analysis and Methods

von den Rohdaten zur 3D VDF

wohin damit?

PHA pro Spin... Ideal / mit Fehlern alpha, beta
, Pile-up, random coincidences/ Schmutztail durch hohe Flüsse
SWICS provides two types of data products from the analogue signals Tof, ESSD and the EPQ-Step. 24-bit

4.1 Data products

PHA words, data transmission

4.1.1 Priority weighting

SWICS performs an on-board mass and mass-per-charge-classification. For every ion with valid measurements the m and mpq are calculated based on the measurements of ESSD, Tof and the particle's EPQ-step using a look-up-table technique.
On the one hand these values are used for sorting the ions into predefined boxes in the m-mpq-space which yield in the so-called matrix rate, a second data product that is provided by SWICS.
Secondly, and more important for our analysis, the m and mpq information is used to sort every measured ion into one of three priority ranges.

Range, BRW

Range 0	$m < 8.7; m_0 : mpq < 3.3$	H, He^+, He^{2+}; Doubles
Range 1	$m > 8.7$	Heavier ions
Range 2	$m_0 : mpq > 3.3$	Doubles

4.1.2 Detection efficiencies

Threshold, Doubles...

4.2 ET matrices, identification

Fig. 4.1 shows longterm PHA data collected with Ulysses SWICS over two years for EPQ Step 25 (= Energy per charge TODO). For every particle with valid measurements the E_{SSD} channel is plotted over the ToF channel. As a particle's mass and mass-per-charge is connected to the measured values EpQ, τ and E_{SSD} by equations

3.1 – 3.3, every ion species occupies a distinct position in the so-called *ET-Matrix*. (Counts of different ion species sum up at distinct places in ... space.)

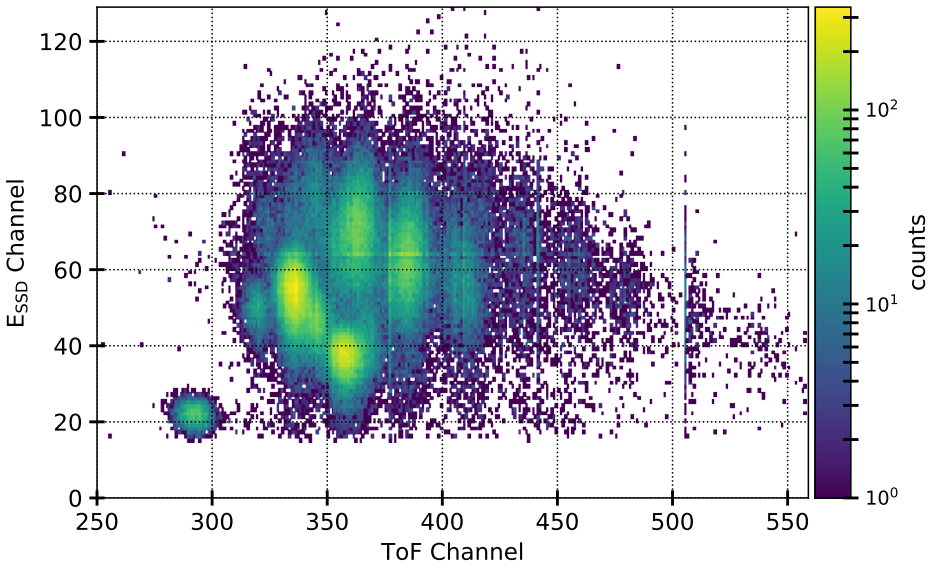

FIGURE 4.1: test

4.3 Filter He+

nominal w based on vsw -> solar wind ions rausfiltern

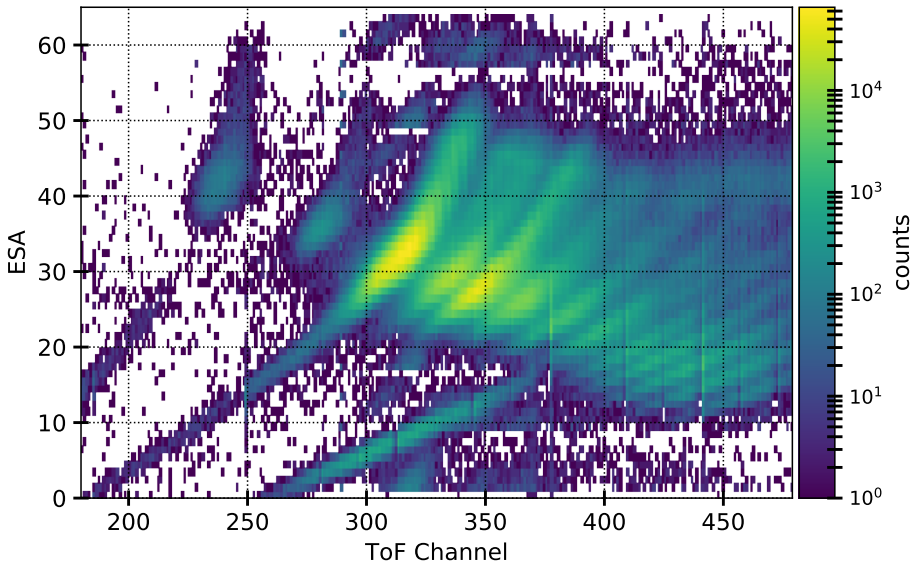

FIGURE 4.2: test

For extracting only the He^+ events from the PHA data we plot the events' energy-per-charge over their measured ToF. Teilchen derselben mpq werden auf Kurven *todo* geortet. Spezies höherer Mpq finden sich auf Kurven mit größeren ToF-Werten.

Man kann so z.B. todo, todo und todo identifizieren. Unten ist He gut zu erkennen weil suprathermal. An die suprathermalen *He*-Teilchen schließen sich zu höheren ToF andere Teilchen mit derselben mpq auf der gleichen Kurve an. Weil die Kurven dort enger liegen, kann man He in dem Bereich auch nicht von anderen mit ähnlicher mpq unterscheiden. We can take advantage of SWICS' on-board priority weighting. We only plot the Range0-events. This roughly cuts out events with $m > 8.7$. Nur H, He2+, He+ bleiben übrig als prominente Ionen. Man sieht, dass auch einige schwerere in die Box reinlecken, aber das betrifft nicht die ESA-Steps, in denen Helium auftritt.
Man kann jetzt prima per Auge eine Maske legen. Zusätzlich w filtern um eventullen Hintergrund zu unterdrücken...? Man sieht, dass wir nur Helium-PHAs bis EpQ-Step todo auswerten. Der Grund ist, dass He1+ aufgrund der geringen Masse nicht genug Energie hat, die Triggerschwelle des SSDs zu überschreiten. Somit liegen He1+-Ionen bei höheren ESA-Steps (kleineren Energien pro Ladung) als Double Coincidences vor und taugen nicht für unsere Analyse.
Für alle Jahre. Anzahl: todo

Plots: Nur RNG0, He und He2 gefiltert. In einem (dann nochmal und Fabrsala synchron) oder einzeln?
Irgendwo He+, He++ und Protonen markieren

4.3.1 Filter He2+

für die spätere Kalibrierung (todo: Verweis) brauchen wir eine Spezies, bei der wir davon ausgehen, dass sie sich mit dem SW-Bulk bewegt und die als Triple Coinzidences vorliegt (für die Richtungsinformation). We choose He2+ wegen guter Statistik und auch in Range0. Im Gegensatz zu He1+ auch bei höheren ESA-Steps anzutreffen, weil mehr Nachbeschleunigung durch die höhere Ladung. Dadurch nicht so schnell unter SSD-Threshold. Gleiches Verfahren, einfach ausschneiden. Hier ist es nicht so wichtig, alles mitzubekommen, weil wir anhand von He2+ keine Analyse der VDF durchführen wollen.
Für alle Jahre. Anzahl: todo

Weitere Daten: vsw von SWOOPS, B-Feld

wie viele Daten bleiben über, wie viele PHA-Worte ca. pro Spin?

4.4 Coordinate Systems

For orientation bla we need coordinate system bla...

4.4.1 Ulysses trajectory, HG system

Todo: Hinweis auf Zeichnung und Kapitel vorne
Trajectory data is used from Ulysses Final Archive (2008) where Ulysses position data on a daily basis is available. The trajectory data is given based on different coordinates, including the heliographic coordinate system in the B1950.0 epoch.

Heliographic Coordinate System:
The heliographic (HG) coordinate system is a Cartesian Sun-centered system with the Sun's equatorial plane as a reference plane. Its X-axis is directed along the line

of ascending node, which is the intersection line of the ecliptic and the solar equatorial plane. While the solar equatorial plane has an inclination of $i_{\odot}7.25°$ against the ecliptic (Fränz and Harper, 2002) the line of ascending node is at a longitude of $\Omega_{\odot} \approx 75°$ relative to the First Point of Aries in 1950 (NASA HelioWeb, 2019). The Z-axis of the HG coordinate system is directed along the Sun's spin axis (northward) and the Y-axis completes the right-handed system.
In HG spherical coordinates the longitude φ_{HG} is defined to be 0° for directions along the X-axis and increases towards the Y-axis. The latitude ϑ_{HG} is 0° for direction within the solar equatorial plane and +90° for northward directions.

When working with the Ulysses trajectory data it was found that these data were given in spherical coordinates for which the $\varphi_{HG} = 0°$ direction was towards $\sim -105°$ longitude relative to the First Point of Aries. This means that the Ulysses trajectory coordinate system is shifted 180° around the solar spin axis against the classical definition (s.a.).
In fig. 4.3 Ulysses' spherical HG coordinates as well its distance from the Sun are given over the time of nearly the complete mission.

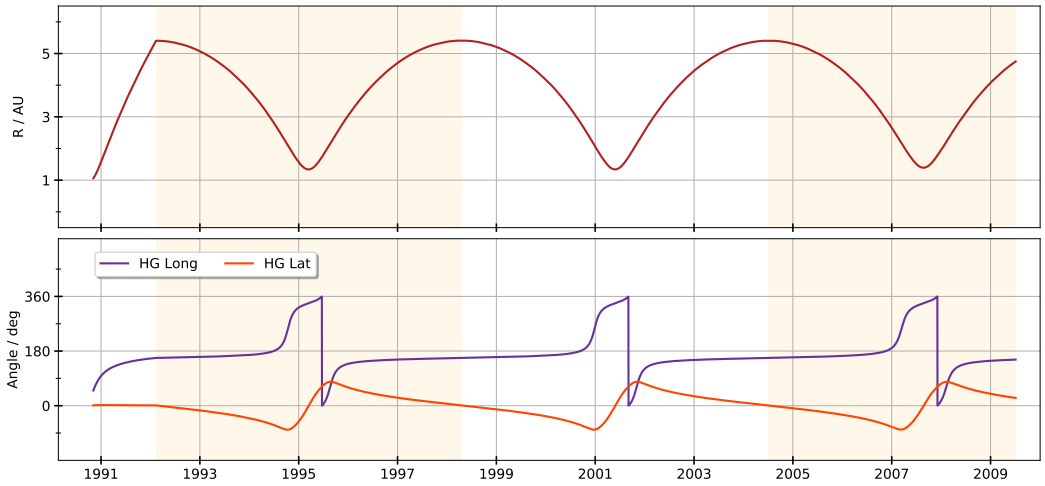

FIGURE 4.3: Ulysses trajectory data from November 1990 to June 2009 based on the data from the Ulysses Final Archive (2008). Color shaded are the three orbits of the mission. **Above:** Shown is Ulysses' radial distance R from the Sun. Perihelion and aphelion of Ulysses' elliptical orbit can clearly be seen as the nearest/farthest distance of 1.3 AU and 5.4 AU. Ulysses passes each of these points every 6.2 years and three times in total over the duration of the mission. **Below:** Shown are Ulysses' heliographic (HG) longitude and latitude. Note, that the longitude is shifted around 180° with respect to the classical definition (s. text for details). A clear periodicity over Ulysses' three orbits can be seen. Maximum and minimum latitude are $\sim \pm 80°$. These points are highest above the poles of the sun and are reached a few weeks before and after Ulysses' pass through the perihelion.

4.4.2 RTN Coordinate System

Umrechnung von HG in RTN?

TODO: The orbit itself is described in heliographic coordinates, so a cs that is constant (stable?) with respect to the sun. For describing positions and velocities in the frame of the spacecraft (e.g. AA) we need another cs...

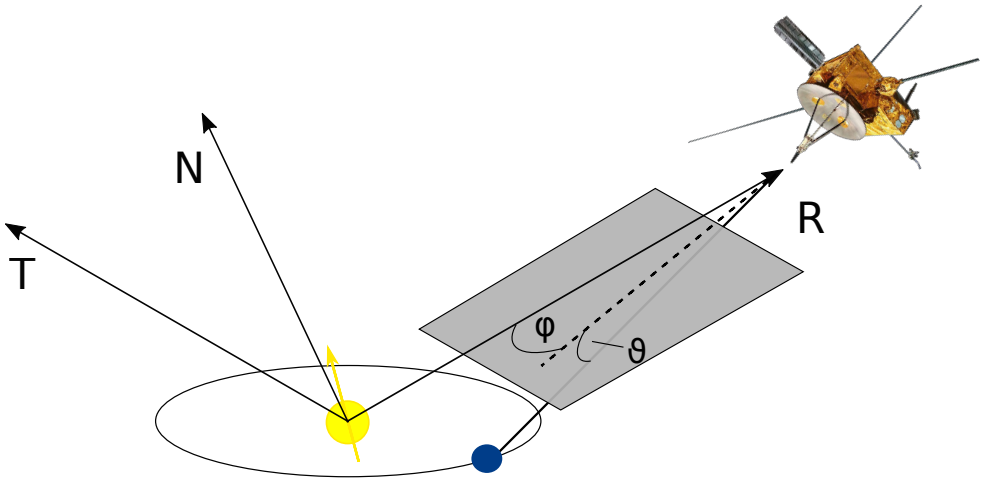

FIGURE 4.4: Graphical representation of the RTN coordinate system (not to scale). Shown are the Sun (yellow), the Earth (blue) and the Ulysses spacecraft at a non-specific position on its orbit. $\vec{R}$ is defined as the unit vector along the line-of-sight Sun–Earth, $\vec{T}$ as the normalized cross product $\vec{\omega}x\vec{R}$ with $\vec{\omega}$ the angular velocity of the Sun (yellow vector). $\vec{N}$ completes the right-handed Cartesian system. Also shown is the definition of the aspect angle components φ_{asp} and ϑ_{asp} as they are used in this work. The grey plane depicts the $\vec{R}$–$\vec{T}$ plane. $0° < \varphi_{asp} < 90°$ and $-90° < \vartheta_{asp} < 0°$ in the shown situation. **TODO: Zeichnung anpassen: Vektorpfeile, Indizes Winkel; Quelle Ulysses Dingsi**

For dealing with Ulysses' trajectory data it is useful to work with *radial-tangential-normal* coordinates. The RTN coordinate system is defined relative to a moving object in the heliosphere – in this case the spacecraft, Ulysses, and is centered at the sun. A graphical representation on the system can be found in fig. 4.4. The unit vectors are $\vec{R}$, $\vec{T}$ and $\vec{N}$, where $\vec{R}$ points radially outward from the sun to the current position of the spacecraft. $\vec{T}$ is defined as the normalized cross product of the Sun's angular velocity $\vec{\omega}$ and $\vec{R}$. $\vec{N}$ completes the right-handed Cartesian coordinate system. Consequently, the RTN system is not defined for a spacecraft's position right above one of the Sun's poles as the cross product $\vec{\omega}x\vec{R}$ is zero here. Nevertheless we do not have to worry about this fact as not even Ulysses crosses the poles directly (todo: Verweis?).

4.5 Collimator/Detector model

Schreiben, dass das eigentlich von ACE/Lars kommt

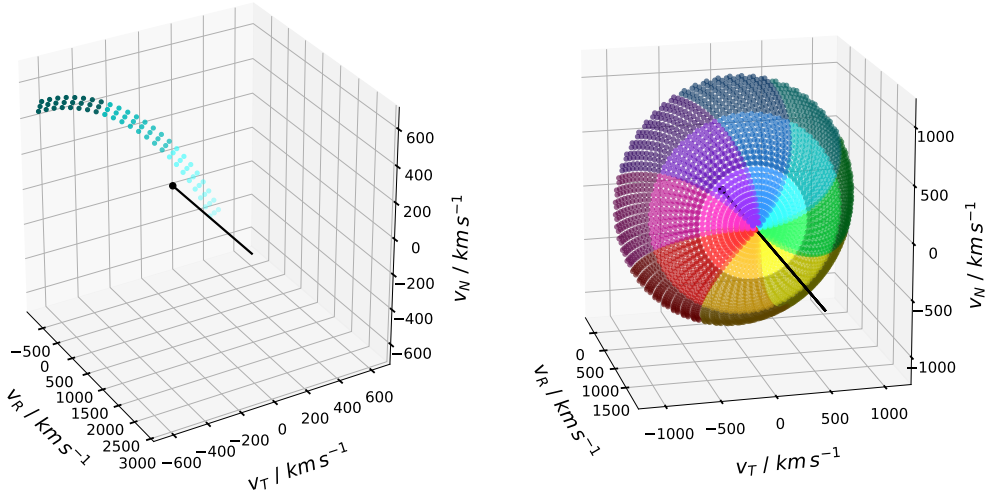

(A) A subfigure (B) A subfigure

FIGURE 4.5: A figure with two subfigures

Motivation

Kollimatormodell – warum eigentlich – wie umgesetzt?

Das Ziel ist, einem gemessenen Teilchen einen v-Vektor zuzuordnen. Eine Sek-Det-Kombi ist aber nicht eindeutig. Ihre Bedeutung hängt davon ab, wohin das Instrument guckt (FoV), von der Eigengeschwindigkeit des SC und davon, wie das SC gerade gedreht ist. Zusätzlich hat der Kollimator eine komplizierte Geometrie, sodass eine analytische Lösung schwierig ist: Also numerische Lösung.
Was macht das Modell? – Ich will das FoV zu jedem Zeitpunkt bestimmen. Ich nehme dafür einzelne Messpunkte auf der originalen Geometrie. Dann gebe ich noch ins Modell, wie das gerade ausgerichtet ist.
Berechnet anhand des AA, wohin Sun trigger schaut, wenn getriggert wird und rotiert coll. an entsprechende Position für Sek 0. Ordnet entsorechend andere Sektoren an. Simuliert FoV durch Punkteraster

4.5.1 Construction

For reconstructing the velocity space that SWICS measures we need to know about the directions of incident particles that can enter the instrument.

The original geometry of the SWICS entrance system, in particular the collimator, was read out from a technical drawing **(TODO: Quelle?!)** Can be described as: Width: Cutting out a hollow piece of 90 deg longitude (**todo: latitude? 4 grad?**) from a sphere (**of r ca. 26 cm ??**) at .. deg polar latitude. The piece is not flat but curved and has a height of ca. 5 cm. This geometry leads to two deflection plates that are curved but have a constant distance of ca. 3.7 cm over a relatively large area which is necessary to provide a constant voltage for the EpQ filtering (s. 3.2.2). Resulting opening angles of the collimator are 69° in width and 4° in height. **Todo: Zeichnung/Abbildung?**
The instrument is mounted with one of the narrow side edges parallel to Ulysses'

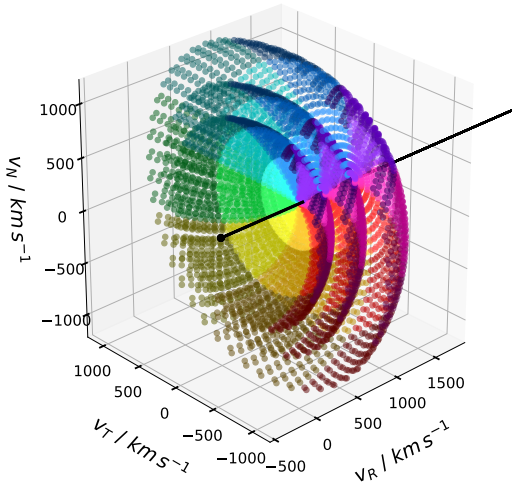

FIGURE 4.6: TODO

spin axis. When we define this edge to lie on the x-axis of a three dimensional Cartesian coordinate system, the collimator geometry can be reconstructed by revolving this edge for 90° around a straight line that lies in the xy-plane with an angle of 56° relative to the x-axis. **Todo: Zeichnung/Abbildung!** Every third of these 90° is reserved as the opening angle for each of the three detector elements, that are described in **Todo**.
The detector's field of view is the solid angle over which the detector is sensitive to incoming particles. It can be represented by a set of outward directed normal vectors on the opening plane of the detector. In our model, we have a variable number of those equidistant vectors both along the width and the height of the detector opening. The real continuous field of view is modelled better with an increasing number of normal vectors that cover the opening. Each of these normalized vectors $\mathbf{f_i}$ has a unique direction $\mathbf{f_i} = \left[f_{x,i}\, f_{y,i}\, f_{z,i}\right]'$ in position space. An example... **(TODO: Plot)**
With a spin of the Ulysses spacecraft the fixedly mounted SWICS instrument is revolves as well around the spacecraft spin axis. Consequently, the field of view is revolved around the x-axis in fig todo. One revolution of SWICS is divided up into eight sectors per 45° each (todo: Verweis auf Instrumentenkapitel oder Erklärung). As the spacecraft is spinning continuously, also the real field of view changes its rotation angle continuously. For our virtual detector we model this by rotating the field of view gradually over n steps through every sector.
The integrated field of view over one spin then comprises TODO single vectors $\mathbf{f_i}$ which are directed symmetrically around the spin axis (s. Abbildung TODO)). In fig. Todo is shown the FoV of todo , you can see a shell with radius 1 bla...

From FoV to Vspace

The detector's velocity acceptance can be calculated by combining the directional information from the field of view and the value of absolute velocity from the current EpQ step.
A particle can only enter the detector when its absolute velocity is within the acceptance of the current EpQ step and when its inverted direction is within the detectors field of view. For a given acceptance velocity v_i and a single field of view vector

$\mathbf{f_i} = \left[f_{x,i}\, f_{y,i}\, f_{z,i}\right]'$ the accepted velocity is

$$\mathbf{v_i} = \begin{bmatrix} v_{R,i} \\ v_{T,i} \\ v_{N,i} \end{bmatrix} = - \begin{bmatrix} f_{x,i} \\ f_{y,i} \\ f_{z,i} \end{bmatrix} \cdot v_i. \tag{4.1}$$

With consideration of the integrated field of view over one spacecraft spin (s.), the acceptance velocity consists of the combination n_todo discrete velocities which form a shell with radius v_i in velocity space. (s. fig. TODO for v_todo)

.

The central velocity for an ion of charge q and mass m for an energy-per-charge step EpQ (in keV/e) is

$$\frac{v_c}{km\,s^{-1}} = \sqrt{\frac{2 \cdot EpQ \cdot 1.60217646 \cdot 10^{-19} \cdot |q|}{m \cdot 1.66053886 \cdot 10^{-27}}}$$

with $m = 4u$ and $|q| = 1$ for He^+.
To represent the uncertainty in EpQ measurement, we take into account the relative uncertainty $\Delta\frac{E}{q}/\frac{E}{q} = \pm 5\%$ and translate it into an uncertainty $\Delta v/v = \frac{1}{2}\left(\Delta\frac{E}{q}/\frac{E}{q}\right) = \pm 2.5\%$ in accepted velocity. For every EpQ step we can now choose a number of i_{epq} single velocities that are distributed evenly in the interval $[v_c - \Delta v/v, v_c + \Delta v/v]$. The total number of accepted velocities v is then $64 \cdot i_{epq}$.
Different absolute velocities v appear as distinct shells of radius v in velocity space. Ein Beispiel, der Übersichtlichkeit halber nur 3 Schalen, ist in bla gezeigt.
With combining all $64 \cdot i_{epq}$ shells we obtain a dense three dimensional pattern of accepted velocities that simulate the real continuous velocity acceptance volume of the spinning detector.

When we measure a PHA word with a distinct SEC, DET and EPQ information, we can now determine its three dimensional velocity with our virtual detector. Of course, the resolution is limited as sector and detector areas are finite as well as the uncertainty $\Delta\frac{E}{q}/\frac{E}{q}$. By spreading the count over the entirety of velocity acceptances in the volume of the SEC DET EPQ combination, we take into account every velocity that could have led to this distinct PHA word.

.

Später schreiben, was für n verwendet wurden

4.5.2 Eigen-velocity

For the considerations in the previous section we assumed a detector on a spacecraft that is fixed in space. Obviously this is not the case for the Ulysses spacecraft (s. sec. TODO) which moves on its elliptical orbit around the Sun.
For determining the spacecraft's velocity we make use of the daily given trajectory

data from sec. TODO. For every time stamp t_i we calculate the spacecraft's instantaneous velocity by forming the differential quotient

$$v_i = \frac{\begin{bmatrix} v_{R,i+1} \\ v_{T,i+1} \\ v_{N,i+1} \end{bmatrix}_i - \begin{bmatrix} v_{R,i} \\ v_{T,i} \\ v_{N,i} \end{bmatrix}_i}{t_{i+1} - t_i}$$

with t_{i+1} being the next time stamp, which is normally $t_i + 1\,\mathrm{d}$. Note, that the spacecrafts position at t_{i+1} has to be considered in the RTN coordinate system that relates to the spacecraft's position at t_i. The resulting velocities in RTN coordinates are shown in fig. todo.
–Bewertung Größenordnung–
To correct the measured velocities for the spacecraft's eigen-velocity, we simply add the resulting velocity components to the velocity acceptance. Thus, for every time stamp the shells (s. fig todo) are shifted a bit in velocity space based on the respective eigen-velocity.

4.5.3 Orientation of the Detector

Until now we have assumed that Ulysses' spin axis is aligned with the R-axis of the coordinate system, i.e. that the spin axis points directly to the Sun. In fact, this is not the case in general. Due to telemetry reasons, Ulysses' high gain antenna has to be oriented directly towards Earth (todo: Vergleich mit ACE, warum?). As Ulysses' spin axis is aligned with the electrical axis of the antenna (Wenzel et al., 1992), has an offset towards the line of sight spacecraft-Sun. This offset is called *aspect angle* and is a permanently changing quantity as a function of Ulysses' position and the position of the Earth. As a varying aspect angle results in SWICS covering different parts of velocity space it is essential to consider this quantity in detail.

Calculation of the Aspect Angle

The aspect angle is measured from the line-of-sight Ulysses–Sun (that is $\vec{R}$) to the line-of-sight Ulysses–Earth. To describe this angle uniquely for any moment, we need two spherical coordinates φ_{asp} and ϑ_{asp} based on the RTN system. As shown in fig. 4.7, φ_{asp} is measured in the $\vec{R}$–$\vec{T}$ plane between $-\vec{R}$ and the projection of the line-of-sight from Ulysses to the Earth into this plane. φ_{asp} is 0° for directions along $-\vec{R}$, that is the line-of-sight from Ulysses to the Sun and increases to positive values towards $-\vec{T}$. ϑ_{asp} is the angle between the projection of the line-of-sight from Ulysses to the Earth into the $\vec{R}$–$\vec{T}$ plane and the line-of-sight itself. It is defined as 0° for directions that lie within the $\vec{R}$–$\vec{T}$ plane and +90° for directions along $\vec{N}$.
(Todo: Lars fragen, ob die genaue Rechnung hier rein muss, Kladde S. 79) For the calculation of the aspect angle we used the Ulysses trajectory data (Verweis ... TODO) and Earth trajectory data in heliographic coordinates on a daily basis from NASA HelioWeb (2019) and converted both to RTN coordinates. In fig. 4.7 both components φ_{asp} and ϑ_{asp} as well as the *flat* aspect angle α with $\alpha = \arccos(\cos\varphi_{asp}) + \arccos(\cos\vartheta_{asp}) - 1$ are shown over the time of the mission. φ_{asp} varies in the range from $\sim -25°$ to $\sim 42°$ and ϑ_{asp} in a range from $\sim -30°$ to $\sim 17°$. Large angles occur especially around the three fast latitude scans, i.e. when Ulysses is at its perihelion and has the smallest distance to Sun and Earth.
(Todo? Beschreiben, dass ich α mit dem Datenprodukt SPE verglichen habe?)

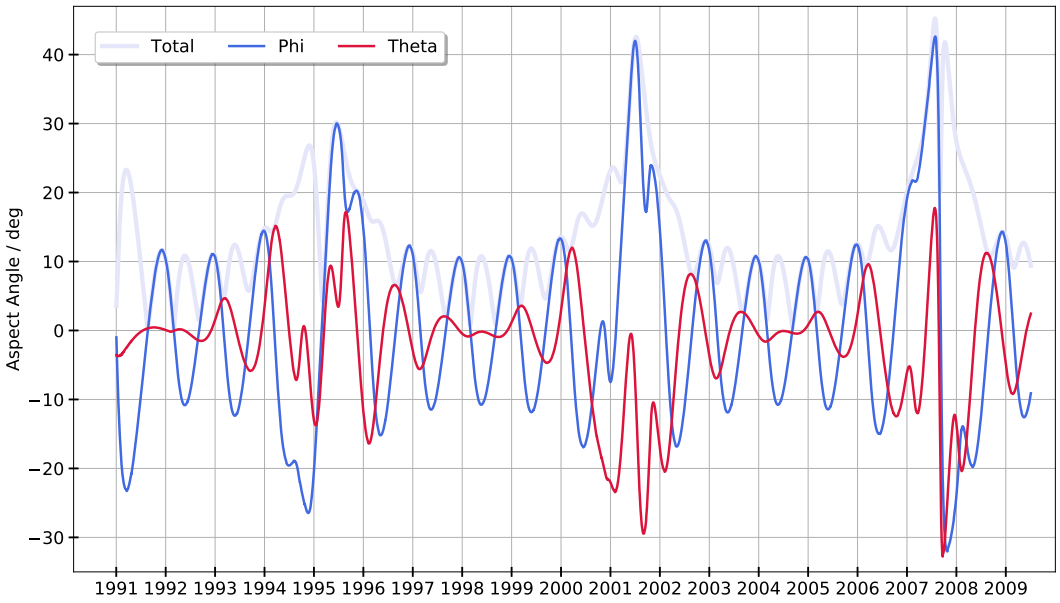

FIGURE 4.7: The evolution of Ulysses' aspect angle components φ_{asp} and ϑ_{asp} from 1991 to the end of the mission are shown. The aspect angle is the angle between the line-of-sight Ulysses–Sun and the orientation of Ulysses' spin axis. A constantly changing aspect angle results from the fact that the spacecraft's antenna, that is nearly parallel with the spin-axis, has to point towards Earth all the time. Particularly large aspect angles occur during the three fast latitude scans around 1995, 2001 and 2007. Here, Ulysses' distance to Sun and Earth is at a minimum. **Also shown is the... (todo: raus aus der Zeichnung?)**

steps asp Winkel

The variable aspect angle is incorporated into the analysis by rotating the field of view corresponding to φ_{asp} and ϑ_{asp}. This results in a likewise rotation of the velocity acceptance space. In fig. todo the acceptance velocity for a single absolute velocity todo is shown for $\varphi_{asp} = todo$ and $\vartheta_{asp} = todo$. Note, that the orientation here seems to be mirrored against the convention that has been described before. This is due to the inversion when transitioning from the field of view to velocity acceptance, s. eq. 4.1.

When comparing fig todo with fig todo, where a situation with $\vartheta_{asp} = \varphi_{asp} = 0$ is shown, it becomes clear that especially larger aspect angles change the link between a distinct sector-detector element and a volume in velocity space. While with a zero aspect angle a radial velocity (along $\vec{R}$) would be detected right in the middle of the velocity shell and definitely in the innermost detector, this is not the case for the aspect angle in fig. todo. Here, an exclusively radial oriented velocity would be detected in a distinct sector in the central detector. (Andersrum bedeutet das, dass eine Sec-Det-Info nur zugeordnet werden kann, wenn die Ausrichtung des Detektors bekannt ist!)

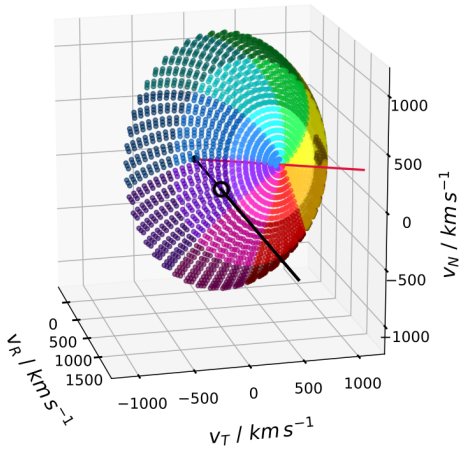

FIGURE 4.8: todo

Probe

For checking if the considerations made before are reasonable and if the virtual detector works in the right way, we want to have a look at data of which we believe to know the VDF. Appropriate test data is the solar wind itself as it is believed to flow radially outwards from the sun (Todo:Quelle). An ideal candidate within the solar wind is He^{2+} as the most abundant species (todo: Quelle). Thus, we can identify He^{2+} easily in fig Todo and are provided with good statistics. Unlike protons, which are even more abundant in the solar wind, He^{2+} most likely deposits energy above the detector's threshold in the SSD detector (s. chap Todo). This is because of its higher mass and the twice as high charge, which leads to a higher gain in energy by the post acceleration (todo:nochmal Verweis?). Only when a particle triggers an ESSD measurement (Triple Coincidence) we get a directional information about its velocity (Verweis todo). Protons are most often measured as Double Coincidences except for suprathermal protons, for which the assumption of radial stream must not hold true (Todo:Quelle). For selecting He^{2+} we proceed like described in chap. todo. Wie viele PHAs sind das dann insgesamt und pro Jahr? Schreiben, dass das nicht so genau gemacht werden musste, weil keine VDF Analyse...

In a first step we look at periods of time in which both aspect angle components φ_{asp} and ϑ_{asp} were small (Todo: genau?). For these nr_todo PHA words we draw a histogram (??) of their sektor and detector information. The result can be seen in fig. todo. The histogram shows that mainly the innermost detector has counts. This is the expected behavior when we imagine the instrument on a spacecraft that points directly to the Sun. A radially streaming flow then hits the instrument's detector that is oriented sunwards. This does not change with the spin of the spacecraft. This result is also consistent with the detector model for $\varphi_{asp} = \vartheta_{asp} = 0$ which is shown in fig. todo. A radial stream can be represented here by the black line which cuts through the velocity shell in its center, the region of the innermost detector, bla. Irgendwie schöner schreiben... (Due to the width... auf allen Sektoren?)

In a second step we take a look at a time period in which Ulysses had a substantial aspect angle. This is particularly the case for when Ulysses is near its perihelion,

s. fig todo. We choose for the second orbit, i.e. days 1-90 (?) in 2001. For all He^{2+} PHA data from this time we again histogram sector and detector information, which is shown in fig. todo. Compared to fig. todo the maximum of counts is now shifted clearly towards a single sector (Nr.?) and the central detector. This is consistent with the virtual detector in fig. todo, where the aspect angle's quantity matches the one in the selected time period. With this orientation a radial stream from the Sun hits the instrument on its center detector and only while a particular moment (?!) of the spin/rotation (?!). Counts do not show up exclusively with this single sector-detector combination but slightly spread out over adjacent sector-detector elements. This is due to the fact that solar wind He^{2+} does not stream as an ideal beam but has a certain width (todo: Referenz).
Verweis: Sektordetails im nächsten Kapitelchen

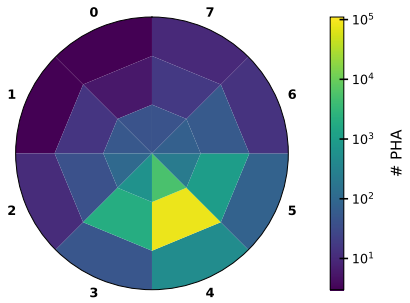

FIGURE 4.9: TODO

Sunpulse Trigger – Rotation

In the previous section hat man gesehen, dass sich die PHA Counts für einen großen AA auf den mittleren Detektor konzentrieren. In diesem Abschnitt soll geklärt werden, wovon es abhängt, in welchem Sektor der Schwerpunkt der Counts landet.

As mentioned before (todo: ist es?), one SC spin is divided into 8 sectors, starting with sector 0 and ending with sector 7. Every spin's start is defined newly by the *spin reference pulse* of Ulysses (Hunt-Ward and Armstrong, 1999).

This pulse is triggered by a combination of four sun sensors which detect when the Sun crosses a plane that is spanned by the spacecraft's spin axis and the spacecraft's x-axis, which is a particular axis perpendicular to the spin axis. The spin reference pulse is not uniform over time as the position of the Sun relative to the spacecraft changes with varying aspect angle.
To extract correct directional information from a sector data product of an ion that has been detected by SWICS it is essential to know the relative orientation between SWICS' main axis and the x-axis on the spacecraft. In the virtual detector this is implemented as an angle against the line-of-sight spacecraft-sun by which the field of view is rotated around the spin axis.
From the SWICS DPU (1988, S.20-22) we know with *normal orientation* the sun pulse occurs in the center of SWICS sector 4, which implies a 180° offset between the line-of-sight spacecraft-sun and SWICS sector 0 (s. fig TODO). However, one can also read that it was possible to set a fine adjustment which would lead to an offset of the sun pulse from this center line up to 22.5° SWICS DPU (1988, S.48). Unfortunately, we do not know about the value that has been chosen.
If we assumed a wrong angle, a particle beam coming from a fixed direction in a

sun-fixed frame would be linked to a different direction. But this shift between true and supposedly measured direction is not constant over aspect angles. If we then measured over a longer time period with various aspect angles, we would measure the beam as blurred in velocity space.
To make sure our model uses the right angle, we again choose He^{2+} as a test population of which we assume a beam-like behaviour streaming radially from the Sun. Also, we can only look at time periods when the aspect angles were large and the maximum of He^{2+} counts occurs in the central or outermost detector. Only here we can clearly discriminate between single sectors. When measured in the innermost detector the slightly widened distribution of He^{2+} would spread across all sectors as they are close together here (s. fig todo). From fig Todo, where we histogrammed bla, we find that the overall idea of a sun pulse in sector 4 should be right when we believe the assumption that He^{2+} streams radially from the Sun. To check for a potential fine adjustment we search for tendencies of the maximum of counts sweeping to an adjacent sector.
Zeigen: Für lange Zeiträume: He2+ kommt zentral. Für einzelne kurze: unterschiedlich. Deshalb: grober Check von wegen Detektor geht gut. Für das Feintuning (180 Grad oder doch was anderes?) reichts aber nicht...
Schemazeichnung SunPulser, dazu Problem irgendwie zeigen

Übergang w

Steps vsw
With the considerations of eigen-velocity and orientation we can now use the virtual detector for displaying velocity distributions of He^{+} pickup ions.

Mithilfe des virtuellen Detektors können jetzt geeignete (Triples) PHA Worte in dreidimensionale Geschwindigkeitskomponenten übersetzt werden (vorher: nur Betrag. Jetzt: Komponenten). Erst mit diesen entfalteten Einzelkomponenten kann man den wichtigen Schritt gehen und in den Sonnenwindframe übergehen. This is done for every PHA word (nein. jeder v-Akzeptanzpunkt in jeden getroffenen Sek-Det-Kombidings...) by subtracting the instantaneous solar wind speed in R-component from the ion's velocity in spacecraft frame:

$$\mathbf{v_{i,sw}} = \begin{bmatrix} v_{R,i,sc} \\ v_{T,i,sc} \\ v_{N,i,sc} \end{bmatrix} - \begin{bmatrix} v_{sw} \\ 0 \\ 0 \end{bmatrix}$$

In a last step every component of the resulting vector is divided the by solar wind speed:

$$\mathbf{w_{i,sw}} = \begin{bmatrix} v_{R,i,sw} \\ v_{T,i,sw} \\ v_{N,i,sw} \end{bmatrix} / \begin{bmatrix} v_{sw} \\ v_{sw} \\ v_{sw} \end{bmatrix}$$

By this, the transition from velocity space in the spacecraft frame to solar wind independent w space in solar wind frame of reference is made.

4.6 VDF

4.6.1 Velocity Space Coverage

When analyzing He^+ PUI w-spectra with Ulysses SWICS, several effects have to be considered that limit the observable part of w-space. The most obvious restriction results from the fixed geometry of the collimator (s. sec todo) which allows to observe only a dome-shaped part of the w-space when considering the spin of the spacecraft and varying EpQ steps. (However, this dome is not fixed in w-space for different orientations of the spacecraft. While the ever changing aspect angle of Ulysses introduces a complex subject to directional data analysis it also enlarges the integrated coverage of velocity space over time.)
Furthermore, we have to deal with a limitation of the coverage in w_R-direction particularly for He^+ triple coincidences. The observable EpQ range for He^+ is limited to TODO to TODO, which corresponds to steps todo to todo. While A is the instrument's highest possible EpQ value, B is the lowest value for which He^+ still has enough energy to overcome the energy threshold of the SSD and thus can trigger a valid energy measurement. The w-range that is consequently covered is highly dependent on the prevalent solar wind speed. For $v_{sw} = 700\,\mathrm{km/s}$ the absolute w in a spacecraft frame is limited to TODO. For slow solar wind at $v_{sw} = 300\,\mathrm{km/s}$ todo... . That means that we are limited to time periods with fast solar wind as we do not expect to measure the bulk of He^+ PUI at w größer als... TODO. In fig. TODO an exemplary w-space coverage for vsw = Todo and no aspect angle is sketched.

Evtl. woanders hin und irgendwie besser schreiben:
In fig. TODO a histogram for occuring solar wind speeds is shown – limited to times in which He^+ triple coincidences were measured. Measured with SWOOPS. The number on the right indicates the total number of He^+ PHA triple coincidence data that was received for that year. One can see the overall variation of the solar wind speed (due to different latitude: slow/fast sw) and that the total number of received data decreases heavily towards years in which Ulysses approaches the orbit's aphelion. This is mainly an effect of pickup ion flux reduction that scales with r^{-2} due to the expansion of the solar wind (Todo:Quelle?).

4.6.2 Phasenraumnormierung

Von Counts zur PSD: Aus den PHA words, die uns Sec, Det und EpQ Info geben (He wissen wir auch) und zusammen mit der Info darüber wie sich das SC gerade bewegt hat und wohin es geguckt hat können wir Counts im 3D w-Raum bestimmen innerhalb der Zeit, die wir gemessen haben.

Die physikalische Größe die wir daraus ableiten wollen ist die PSD.

Phasenraumdichte in einzelnem Det-Sec-Epq-Element (Annahme: übers ganze Element konstant. Oder ich nehm die mittlere Dichte):

V: spatial volume of the measurement (G: geometry factor)

$$\begin{aligned} N_{ijk} &= \iiint\limits_{v_{\varphi i} v_{\vartheta j} v_{Rk}} \rho_{ijk} V_k \; d^3v \\ &= \iiint\limits_{v_{\varphi i} v_{\vartheta j} v_{Rk}} \rho_{ijk} \, G \, v_k \, \tau \; d^3v \\ &= v_k^2 \left(\frac{\pi^2}{180^2} \cdot 4 \cdot 69 \right) \Delta v_k \, \rho_{ijk} \, G \, v_k \, \tau \\ &= v_k^4 \left(\frac{\pi^2}{180^2} \cdot 4 \cdot 69 \right) 0.025 \, \rho_{ijk} \, G \, \tau \end{aligned}$$

Effizienz; Aufteilen auf die großen w-Bins...

Detection Efficiency

(Frage Lars: Welche Wahrscheinlichkeit genau gibt die E. an? Ausgehend von einem Teilchen vor dem Instrument mit der richtigen Epq? Von einem Teilchen, das den EpQ Filter durchlaufen hat?)

The detector efficiency is the probability to measure a particle that has entered the instrument(?). When working with SWICS, like for any physical measurement, one has to consider several effects that impede the ideal measurement as it is described in sec. todo. These effects are highly dependent from the ion species and deflection step and include for example that secondary electrons for the time of flight measurement (in carbon foil and SSD) may not be emitted properly. Also, ions could pass through the time of flight section on divergent trajectories due to scattering processes (in the carbon foil??). Possibly, the ion then does not hit the sensitive area of the SSD and does neither trigger a stop signal for the time of flight measurement nor a valid energy measurement in the SSD. Even for an ion that hits the SSD centrally

Another reason for a missing energy deposit in the SSD is that the ion's energy is smaller than the threshold of the SSD. The reason for choosing a nonzero threshold is to limit the influence of the SSDs natural noise. For SWICS this noise level is quite high (todo: Quelle!! Goldfolie?) so that the threshold is chosen to be TODO. Ions with a small mass and charge are most likely to not overcome the threshold. For He^+ this is already the case for deflection step TODO that corresponds to a He^+ velocity of TODO (s. sec TODO). Unfortunately, He^+ detection efficiencies are not known to us for Ulysses SWICS. Instead, we make use of the efficiencies from ACE SWICS (todo: woher?). As ACE SWICS uses different EpQ deflection steps and seems to have a different SSD threshold we extrapolated the values for Ulysses SWICS. For the highest EpQ value TODO we interpolated the efficiency from the ACE triple efficiencies and then extrapolated linearly to an efficiency of 0 at EpQ step 17. By this, we accommodate for the fact that He^+ does not have enough energy to deposit energy above the SSD threshold at step TODO and thus, the probability for a triple coincidence is zero (Todo: Verweis auf anderes Kapitel: Coverage). He^+ efficiencies from ACE SWICS and the resulting efficiencies used for Ulysses SWICS are shown in fig. TODO. For sure, these values are not realistic but represent the overall trend of a decreasing efficiency for higher EpQ steps at least.

.

Mittlere Phasenraumdichte in einem Bin, in den zwei Instrumentenbins A und B reingehen: (differential PSD)

$$\bar{\rho} = \frac{N_A + N_B}{\frac{N_A}{N_{A,ges}} V_A + \frac{N_B}{N_{B,ges}} V_B} \tag{4.2}$$

Dabei ist N_i die Anzahl der Hits, die im Messbin gelandet sind und $N_{i,ges}$ die gesamte Anzahl an Bins. Hits heißt GEsamtcounts durch Detektoranzahl. Eigentlich gebe ich statt N_i $N_i \cdot Detektoranzahl$ rein, aber das kürzt sich ja raus.

Effizienz und Sektorgewichte dazu:
Allg.:

$$\rho = \frac{N \cdot brw}{V \cdot Eff}$$

Und dann

$$\bar{\rho} = \frac{N_A + N_B}{\frac{N_A}{N_{A,ges}} \frac{V_A \cdot eff_A}{brw_A} + \frac{N_B}{N_{B,ges}} \frac{V_B \cdot eff_B}{brw_B}} \tag{4.3}$$

Unsicherheit EpQ: Delta v. Rechnung fehlerfortpflanzung Kladde S. 84

4.7 Und dann so

Ich hab jetzt ein Set von v-Komponenten pro PHA-Event. Daraus kann ich berechnen: (mit: In Komponenten aufgeteilt kann man jetzt Geschwindigkeit im SW-frame berechnen, indem man vsw in R-Richtugn abzieht)

- Betrag im SW frame
- Winkel im w-space (SW frame)

B-Feld. Von welchem Instrument? auch RTN-System. Genauso Winkel berechnet.
1-min-Mittel (Gyroradius Zeit zeigen) und entsprechend EpQ-Steps den PHAs zugeordnet.

4.8 Results

4.8.1 Slices

4.8.2 Skymaps

4.8.3 1D

4.9 Outlook

- Efficiency müsste genau bestimmt werden: Dabei berücksichtigen, welcher Anteil unter den Threshold wandert. Evtl. überschätzen wir die Eff., wenn wir die interpolierten Werte von ACE/SWICS nehmen.
- B-Feld-spezifische Untersuchung: Torus

- Radialabhängigkeit: adiabatic Cooling, PA-Scattering
- Sonnenwindanalyse: Ist zu breit. In Richtung Spin-Achse könnte man aber über die Schalen analysieren (Lars fragen: radial?)

4.9.1 Loose Ends

- andere Daten: B, vsw (Swoops: als vsw wird Protonengeschw. genommen. Ist das überhaupt richtig, ist das der Referenzframe? Und Annahme, dass vsw rein radial ist)
- Die Sache mit dem BRW ab 2003
- Englisch: Relativpronomen, Kommasetzung, British/American
- He^{1+} einheitlich, mathrm
- Tempus?
- kursiv / nicht kursiv wie war das nochmal

Bibliography

Allegrini, F., N. A. Schwadron, D. J. McComas, G. Gloeckler, and J. Geiss (May 2005). "Stability of the inner source pickup ions over the solar cycle". In: *Journal of Geophysical Research* 110.A5, A05105, A05105. DOI: 10.1029/2004JA010847.

Drews, Christian, Lars Berger, Andreas Taut, Thies Peleikis, and Robert F. Wimmer-Schweingruber (Mar. 2015). "2D He^+ pickup ion velocity distribution functions: STEREO PLASTIC observations". In: *Astronomy & Astrophysics* 575, A97, A97. DOI: 10.1051/0004-6361/201425271.

European Space Agency (2019). *ESA Website – Ulysses Orbit*. URL: https://www.cosmos.esa.int/web/ulysses/the-ulysses-orbit (visited on 10/27/2019).

Fränz, M. and D. Harper (Feb. 2002). "Heliospheric coordinate systems. Corrected Version". In: *Planetary & Space Science* 50.2, pp. 217–233. DOI: 10.1016/S0032-0633(01)00119-2.

Frisch, Priscilla C., Seth Redfield, and Jonathan D. Slavin (Sept. 2011). "The Interstellar Medium Surrounding the Sun". In: *Annual Review of Astronomy and Astrophysics* 49.1, pp. 237–279. DOI: 10.1146/annurev-astro-081710-102613.

Geiss, J., G. Gloeckler, L. A. Fisk, and R. von Steiger (1995). "C+ Pickup ions in the heliosphere and their origin". In: *Journal of Geophysical Research: Space Physics* 100.A12, pp. 23373–23377. DOI: 10.1029/95JA03051. eprint: https://agupubs.onlinelibrary.wiley.com/doi/pdf/10.1029/95JA03051. URL: https://agupubs.onlinelibrary.wiley.com/doi/abs/10.1029/95JA03051.

Geiss, J., G. Gloeckler, and R. von Steiger (Apr. 1995). "Origin of the solar wind from composition data". In: *Space Science Reviews* 72.1, pp. 49–60. ISSN: 1572-9672. DOI: 10.1007/BF00768753. URL: https://doi.org/10.1007/BF00768753.

Gloeckler, G., L. A. Fisk, J. Geiss, N. A. Schwadron, and T. H. Zurbuchen (Apr. 2000). "Elemental composition of the inner source pickup ions". In: *Journal of Geophysical Research* 105.A4, pp. 7459–7464. DOI: 10.1029/1999JA000224.

Gloeckler, G., J. Geiss, H. Balsiger, P. Bedini, J. C. Cain, J. Fischer, L. A. Fisk, A. B. Galvin, F. Gliem, D. C. Hamilton, J. V. Hollweg, F. M. Ipavich, R. Joos, S. Livi, R. A. Lundgren, U. Mall, J. F. McKenzie, K. W. Ogilvie, F. Ottens, W. Rieck, E. O. Tums, R. von Steiger, W. Weiss, and B. Wilken (Jan. 1992). "The Solar Wind Ion Composition Spectrometer". In: *Astronomy & Astrophysics Supplement Series* 92.2, pp. 267–289.

Gloeckler, G., N. A. Schwadron, L. A. Fisk, and J. Geiss (Jan. 1995). "Weak pitch angle scattering of few MV rigidity ions from measurements of anisotropies in the distribution function of interstellar pickup H^+". In: *Geophysical Research Letters* 22.19, pp. 2665–2668. DOI: 10.1029/95GL02480.

Hunt-Ward, T. and T.P. Armstrong, eds. (1999). *Ulysses HISCALE Data Analysis Handbook*. Fundamental Technologies, LLC.

Möbius, E., D. Hovestadt, B. Klecker, G. Scholer, and G. Gloeckler (1985). "Direct observation of He+ pick-up ions of interstellar origin in the solar wind". In: *nature* 318 (6045), pp. 426–429. DOI: 10.1038/318426A0.

Möbius, E., D. Rucinski, M. A. Lee, and P. A. Isenberg (Jan. 1998). "Decreases in the antisunward flux of interstellar pickup He^+ associated with radial interplanetary

magnetic field". In: *Journal of Geophysical Research* 103.A1, pp. 257–266. DOI: 10.1029/97JA02771.

NASA HelioWeb (2019). *Heliocentric Trajectories for Selected Spacecraft, Planets, and Comets*. URL: https://omniweb.gsfc.nasa.gov/coho/helios/heli.html (visited on 06/01/2019).

Oka, M., T. Terasawa, H. Noda, Y. Saito, and T. Mukai (June 2002). "'Torus' distribution of interstellar helium pickup ions: Direct observation". In: *Geophysical Research Letters* 29.12, 1612, p. 1612. DOI: 10.1029/2002GL015111.

Prölss, Gerd W. (2004). *Physik des erdnahen Weltraums. Eine Einführung*. Springer Berlin Heidelberg. DOI: 10.1007/978-3-642-18807-7.

Schwadron, N. A., J. Geiss, L. A. Fisk, G. Gloeckler, T. H. Zurbuchen, and R. von Steiger (Apr. 2000). "Inner source distributions: Theoretical interpretation, implications, and evidence for inner source protons". In: *Journal of Geophysical Research* 105.A4, pp. 7465–7472. DOI: 10.1029/1999JA000225.

Schwadron, N. A., E. Möbius, T. Leonard, S. A. Fuselier, D. J. McComas, D. Heirtzler, H. Kucharek, F. Rahmanifard, M. Bzowski, M. A. Kubiak, J. M. Sokół, P. Swaczyna, and P. Frisch (Oct. 2015). "Determination of Interstellar He Parameters Using Five Years of Data from the IBEX: Beyond Closed Form Approximations". In: *The Astrophysical Journal Supplement Series* 220.2, 25, p. 25. DOI: 10.1088/0067-0049/220/2/25.

SWICS DPU (1988). Ed. by F. Gliem, W. Rieck, and H. Dinse.

Ulysses Final Archive (2008). Ed. by European Space Agency. URL: http://ufa.esac.esa.int/ufa/#data (visited on 08/01/2019).

Vasyliunas, V. M. and G. L. Siscoe (1976). "On the flux and the energy spectrum of interstellar ions in the solar system". In: *Journal of Geophysical Research (1896-1977)* (7).

Wenzel, K. P., R. G. Marsden, D. E. Page, and E. J. Smith (Jan. 1992). "The ULYSSES Mission". In: *Astronomy and Astrophysics Supplement* 92, p. 207.

Wimmer-Schweingruber, R. F. and P. Bochsler (May 2002). "On the Origin of Inner-Source Pickup Ions". In: *Geophysical Research Letters* 30.2, pp. 49-1 - 49-4.

Declaration of Authorship

I, Anne Fischer, declare that this thesis titled, and the work presented in it are my own. I confirm that:

- This work was done wholly or mainly while in candidature for a research degree at this University.
- Where any part of this thesis has previously been submitted for a degree or any other qualification at this University or any other institution, this has been clearly stated.
- Where I have consulted the published work of others, this is always clearly attributed.
- Where I have quoted from the work of others, the source is always given. With the exception of such quotations, this thesis is entirely my own work.
- I have acknowledged all main sources of help.
- Where the thesis is based on work done by myself jointly with others, I have made clear exactly what was done by others and what I have contributed myself.

Signed:

Date:

Acknowledgements

The acknowledgments and the people to thank go here, don't forget to include your project advisor…